Cortico-basal oscillations index naturalistic movements during deep brain stimulation

Daryl Lawrence,[1] Guy Avraham,[2,3] Jiaang Yao,[1] Lexin Li,[4] Chengchun Shi,[5] Philip A. Starr[6] and Simon J. Little[3]

Abstract

The basal ganglia and sensorimotor cortex are essential nodes of a network that supports motor control. In Parkinson's disease, disruptions in this network lead to rigidity and slowness during movement execution. Deep brain stimulation (DBS) of the basal ganglia has proven effective in alleviating Parkinson's disease-related hypokinetic symptoms, and sensing-enabled neurostimulators now afford the opportunity to detect cortico-basal oscillations during motion. However, the specific contributions of these motor network nodes to chronic, naturalistic movement and the effects of DBS on circuit dynamics are not well understood.

To address these gaps, we recorded over 530 hours of cortical and subcortical signals from 15 Parkinson's disease patients (27 hemispheres) during unsupervised, unconstrained daily activities and subthalamic or pallidal DBS. Synchronized wrist-worn accelerometers tracked forearm speeds, supporting the evaluation of neural biomarkers related to motion. Our study validated and extended the known relationship between cortical and subcortical beta power (13 – 30 Hz) and movement. We show that cortical low (13 – 20 Hz) and high (21 – 30 Hz) beta movement-related desynchronization (MRD) effectively distinguished between mobile and stationary states. In the subthalamic nucleus (STN) and globus pallidus interna (GPi), high beta MRD and gamma (40 – 80 Hz) movement-related synchronization (MRS) exhibited significant group-level correlations with movement kinematics. When stimulated at 130 Hz, cortical stimulation-entrained gamma oscillations at the half-harmonic (~65 Hz) were observed. Further, cortical entrained gamma MRS was a stronger predictor of motion than broadband gamma MRS.

We developed machine learning (ML) models to predict naturalistic movement over extended periods using spectral features from brief neural recordings (0.5 – 8 s epochs). Cortical models outperformed subcortical models, although combining cortico-basal signals yielded the highest model performance (AUC > 0.85 for binary movement state classifiers; Pearson *r* statistic > 0.68 for continuous forearm speed regressors). Higher DBS

current amplitudes were associated with reduced beta MRD and low gamma (40 – 60 Hz) MRS in the STN/GPi. This negatively impacted the accuracy of the subcortical models, whereas cortical and cortico-basal model performance remained stable across stimulation amplitudes.

Our study demonstrates that cortico-basal nodes of the motor network encode complementary kinematic information, which can be integrated to enhance the accuracy and stability of chronic, naturalistic movement decoding during deep brain stimulation. These insights support the development and integration of therapeutic brain-computer interfaces (BCIs) with closed-loop, adaptive DBS (aDBS) to leverage rapid and precise movement-predictive models for the treatment of motor network disorders.

Author affiliations:

1 University of California, Berkeley – University of California, San Francisco Graduate Program in Bioengineering, Berkeley, CA 94720, USA

2 Department of Psychology, University of California, Berkeley, Berkeley, CA 94720, USA

3 Department of Neurology, University of California, San Francisco, San Francisco, CA 94143, USA

4 Department of Public Health, University of California, Berkeley, Berkeley, CA 94720, USA

5 Department of Statistics, London School of Economics and Political Science, London, WC2A 2AE, UK

6 Department of Neurosurgery, University of California, San Francisco, San Francisco, CA 94143, USA

Correspondence to: Daryl Lawrence

UCSF Joan and Sanford I. Weill Neurosciences Building

University of California, San Francisco

1651 4th St, Room 383C

San Francisco, CA 94158, USA

E-mail: daryl.lawrence@ucsf.edu

Running title: Cortico-basal biomarkers of movement

Keywords: sensorimotor cortex; basal ganglia; intracranial electrodes; deep brain stimulation; movement disorders; brain-computer interfaces

Introduction

Precise motor control is essential for executing autonomous and volitional movements.[1] The basal ganglia and sensorimotor cortex are integral nodes of the motor network that operate together to enable accurate, well-coordinated movements.[2,3] Within the basal ganglia circuitry, the subthalamic nucleus (STN) and globus pallidus internus (GPi) regulate movement by selecting amongst competing motor programs and relaying information to the cortex.[4–6] The sensorimotor cortex is generally responsible for planning and executing voluntary movements via neuronal projections to the brainstem and spinal cord.[7,8] The basal ganglia and sensorimotor cortex may provide complementary information and perform distinct roles in coordinating motor activity although the specific neural dynamics underlying this relationship are not yet well-established.[9,10]

Laboratory-based recordings of local field potentials (LFPs) from the basal ganglia and sensorimotor cortex have identified potential neurophysiological biomarkers linked to kinematic features.[11,12] In the subthalamic nucleus (STN), a reduction in beta power (12 – 30 Hz) and an increase in broadband gamma power (55 – 90 Hz) are associated with elevated motor vigor in constrained, ballistic motor tasks.[13–16] In the sensorimotor cortex, a decrease in alpha and beta power, along with an increase in broadband gamma power, have been observed during motor planning and execution.[17,18] While these findings provide insights into movement-related spectral changes, they are primarily based on neural data recorded during brief, supervised, highly-controlled tasks in perioperative settings. Reliable long-term intracranial decoding of human motion, in naturalistic environments over extended periods has not yet been achieved. Identifying the cortical and subcortical biomarkers of real-time movement is essential for understanding the specific contributions of each node of the motor network to the execution of selected motor plans.[19]

Impairment of the motor network leads to movement disorders, such as Parkinson's disease and essential tremor, which are debilitating and often challenging to treat.[20] While open-loop deep brain stimulation (DBS) has proven effective, particularly for Parkinson's disease, its efficacy is limited by fluctuations in symptom severity and medication levels.[21] New technological advancements, including brain-computer interfaces (BCI) and closed-loop, adaptive deep brain stimulation (aDBS), present promising opportunities for

developing personalized treatments with greater therapeutic benefit. Historically, these technologies have been developed independently, with BCIs focusing on precise neural signal decoding and aDBS targeting clinically-defined states (e.g. fluctuations in dopaminergic medication levels) or underlying physiology (e.g. beta bursts).[22,23] However, given the core deficit of movement disorders, we investigate an approach that integrates these techniques, BCI-aDBS. The main concept here is to detect a patient's intention to move from intracranial brain signals and rapidly ramp up DBS at that moment to support motor execution.

Recently, our group demonstrated the proof-of-principle of this BCI-aDBS method in a single Parkinson's disease patient.[24] We developed aDBS policies that targeted movement during brief, constrained motor tasks. This study demonstrated accurate cortically-based movement decoding and improved hand speeds during a keyboard typing task with a reduction in involuntary, dyskinetic movements during rest. However, the neural biomarkers of continuous, unconstrained movement remain undetermined, hindering the development of personalized, movement-responsive BCI-aDBS therapies for disorders of movement at scale.[25]

A new generation of neurostimulators for DBS have been developed that can record neural activity while delivering electrical current to the basal ganglia.[22,26] These recordings can be collected in naturalistic environments, providing an ideal platform to investigate the complementary roles of the basal ganglia and cortex in movement. We recorded 539 hours of cortical and subcortical signals from a cohort of Parkinson's disease patients (15 patients; 27 independent hemispheres) implanted with neurostimulators while they performed unconstrained activities of daily living at home during therapeutic DBS. Wrist-worn accelerometers were used to track forearm speeds of patients and synchronized to neural recordings.[27,28] We identified site-specific neural signals related to motion and developed machine learning (ML) models for movement prediction. Furthermore, we leveraged these findings to elucidate the effects of varying the stimulation amplitude on movement decoding, ML performance and site-specific kinematic biomarkers.

Materials and methods

Participant selection and assessment

We enrolled 15 individuals (mean age: 63 ± 3 years) with idiopathic Parkinson's disease from the movement disorders surgery clinic at the University of California, San Francisco (UCSF) in accordance with the declaration of Helsinki **(Table 1)**. The study was reviewed by the UCSF Institutional Review Board (ClinicalTrials.gov: NCT03582891) under an

investigational device exemption (G180097/R003) for the Summit RC+S device (Medtronic, Inc.).[21] These patients presented with standard clinical indications for STN (12 patients) or GPi (3 patients) deep brain stimulation as confirmed by a movement disorders neurologist following the criteria outlined by the Movement Disorders Society for Parkinson's disease diagnosis. The patients' motor function prior to implantation was assessed using the Unified Parkinson's disease Rating Scale (UPDRS) Part III and their cognitive abilities were evaluated through the Montreal Cognitive Assessment (MoCA). Participants with a MoCA score of 20 or below, or those with an untreated mood disorder as determined by a neuropsychologist, were excluded from the study.

Surgical implantation

Quadripolar depth leads were surgically inserted into either the subthalamic nucleus (Medtronic 3389 lead) or the globus pallidus internus (Medtronic 3387 lead).[29] Electrocorticography (ECoG) strips, designed solely for sensing purposes, were positioned along a parasagittal trajectory to ensure that at least one contact aligned with both the precentral and the postcentral gyri.[22] The precise locations of these electrodes were determined intraoperatively using cone beam computed tomography (CT) fused to preoperative MRI scans. The cortical and subcortical leads were connected to a Summit RC+S implantable pulse generator (model B35300R) above the ipsilateral pectoralis muscle via 60-cm lead extenders (model 37087).[30]

Intracranial data acquisition and preprocessing

We collected over 530 hours of neural data while patients performed unsupervised unconstrained activities of daily living at home (May 2020 – May 2023) **(Fig. 1A)**.[22,31] Baseline recordings were performed in 7 of the 15 patients at a stimulation amplitude of 0 mA, prior to the initiation of DBS therapy, to establish the patients' initial motor symptom profiles. As part of clinical care, a movement disorders specialist identified the optimal DBS electrode contacts and stimulation amplitude to maximize therapeutic benefit while minimizing side effects, such as dyskinesia. 11 patients were recorded at various stimulation amplitudes during the DBS parameter optimization phase.

Throughout the study, participants continued taking their prescribed antiparkinsonian medications as per clinical guidance from their treating neurologist. ECoG leads captured neurophysiological data from the primary motor (M1) and somatosensory (S1) cortices, while depth leads recorded signals from the STN or GPi. The precise locations of these cortical and subcortical electrodes were reconstructed using the *Locate Electrodes Graphical User Interface* toolbox **(Fig. 1B)** and *Lead-DBS* toolbox **(Fig. 1C)** respectively. The neural data was recorded at a sampling frequency of 250 or 500 Hz and transmitted from

the RC+S neurostimulator devices to a nearby telemetry module then to a Microsoft Windows tablet. The tablet was equipped with custom software**,** built on the Summit RC+S application, developed in compliance with FDA regulations (CFR 820.30) and available athttps://github.com/openmind-consortium.

Cortical and subcortical local field potentials recorded by the RC+S devices were first preprocessed in *MATLAB R2022b* using the *Analysis-rcs-data* toolbox **(Fig. 1D)**.[32] They were then filtered from 0.8 – 100 Hz with an infinite impulse response (IIR) elliptic bandpass filter (1dB passband ripple; 100 dB attenuation). For artifact detection and removal, we squared the magnitude of the neural signals and performed Gaussian smoothing over a moving 1-s window. Amplitudes exceeding five times the median were identified as aberrant spikes and the time series corresponding to these periods were removed. Removal of ECG artifacts was carried out utilizing two *MATLAB* libraries, *Perceive* and *PerceptHammer*.[33,34] *Perceive* detected QRS-like patterns within 10-minute intervals (to accommodate variations in ECG artifacts over time).[33] These patterns were then averaged within each session and employed as initializations for the template subtraction pipeline from the *PerceptHammer* library.[34] The initial template facilitated the identification of ECG artifact locations within the underlying signal, and this template was continuously updated using Woody's adaptive filter. However, this recursive process of artifact identification and template updating had the potential to transform the template into one that matched non-artifactual low-frequency spectral power, leading to inaccurate template subtraction. To mitigate this issue, we constrained the transformation of the initial template by comparing the updated and initial templates via normalized cross-correlation. If the cross-correlation between templates fell below a threshold of 0.9, the initial template was utilized for the entire artifact identification and subtraction process without iterative modification by the adaptive filter.

Accelerometry data acquisition and preprocessing

Participants wore an Apple Watch (Apple Inc.) on the wrist contralateral to the hemisphere where the RC+S device was implanted. For patients with bilateral implants, two watches were worn to simultaneously record movement in both forearms at a sampling rate of 50 Hz.[24] Accelerometry data was transmitted from the watches to nearby iPhones through the StrivePD iOS application (Rune Labs Inc.). Previously-validated external algorithms generated tremor and dyskinesia scores at 1-minute intervals.[35] Accelerometry signals in the x, y, and z directions were integrated to derive the respective velocity measurements, filtered between 0.2 and 10 Hz using a fourth-order Butterworth bandpass filter. The resulting x, y, and z velocities were used to compute absolute forearm speeds.

Statistics

For our statistical analyses, we utilized various *Python* (v3.9.17) packages, including *SciPy and Statsmodels*. One-way analyses of variance (ANOVAs) were utilized to explore significant differences between the means of two or more groups. Wilcoxon signed-rank tests were employed for the non-parametric comparison of paired samples. All relevant *p*-values underwent correction for multiple comparisons through the false discovery rate (FDR) procedure.[36] Linear mixed models (LMMs) were constructed utilizing the *Pymer4* library, with individual patients and hemispheres considered as random effects. These LMMs were employed to examine the influence of stimulation current amplitude on neural biomarkers and movement-predictive models' performance.

Power spectral analyses

Cortical and subcortical power spectra were computed from the preprocessed LFPs using a one-dimensional Fourier Transform in the NumPy package (*numpy.fft.fft*) **(Fig. 1E)**. The neural signals were divided into non-overlapping 0.5-second epochs, and a Hann window was applied to calculate power spectral densities (PSDs) ranging from 0 – 100 Hz and spanning 2 Hz each **(Fig. 1F)**. To eliminate the aperiodic component in each power spectrum, the spectral parameterization (SpecParam) algorithm was employed across the 4 – 100 Hz range **(Fig. 1G)**.[37,38] To minimize the impact of involuntary movements on our analyses, we excluded epochs that had a non-zero tremor or dyskinesia severity score, as these scores indicated the presence of symptoms of significant severity.[35] The RC+S and Apple watch devices were set to computer clock time based on the network time protocol to synchronize the timestamps from both devices. As an added step, we identified the time lag between their clocks that maximized the cross-correlation of their respective accelerometry measurements.[39] Once the timestamps were aligned, we linearly interpolated the wearable accelerometry data to determine the absolute forearm speed for each 0.5-second segment.

We combined forearm speed measurements from all patients to produce a group-level distribution and identified a local minimum to be used as a standardized threshold for distinguishing between periods of movement (mobile states) and rest (stationary states) **(Fig. 1H)**. We labelled epochs based on their movement states and calculated Cohen's d (Cd) effect sizes using their power spectral densities (PSDs), adjusting for class imbalances with pooled standard deviations **(Fig. 1I)**.[40] The Cd values provided a signed, normalized metric to quantify the discriminative differences between the flattened PSDs in the mobile or stationary states. Additionally, we computed Spearman's ρ, a non-parametric measure that is robust to outliers, to examine the correlation between the PSDs from each brain region and the contralateral absolute forearm speed measurements.

Machine learning model development and evaluation

We developed linear and non-linear classifiers and regressors using the *Python*-based *scikit-learn* (*sklearn*) library to distinguish between mobile and stationary states or predict absolute forearm speeds respectively. Prior to model training, we standardized the data by removing the mean and scaling it to unit variance. To evaluate the performance of the classifiers, we used the area under the receiver operating characteristic curve (AUC) as our primary metric. AUC is robust to class imbalance making it particularly effective for evaluating model performance across various decision thresholds.[41,42] Moreover, we calculated accuracies, F1-scores, and positive predictive values, as secondary metrics. To balance our training datasets, we used the Synthetic Minority Over-sampling Technique (SMOTE).[43] For the regression analysis, we assessed model performance using the Pearson correlation coefficient (*r* statistic) to compare true and predicted speed values.[44] As a secondary metric, we employed the mean squared error.[45]

To reduce both multicollinearity and complexity, we calculated six canonical power bands (PBs) to serve as features for our linear models: alpha (8 – 12 Hz), low beta (13 – 20 Hz), high beta (21 – 30 Hz), low gamma (40 – 60 Hz), stimulation-entrained gamma (63 – 67 Hz), and high gamma (70 – 90 Hz). In addition, we employed principal component analysis (PCA) to generate subject-specific features. This approach enabled a direct comparison between the effectiveness of canonical PBs versus personalized principal components (PCs) for predicting movement. For more complex non-linear models, we utilized the complete set of PSDs as features without any dimensionality reduction.

For the classifiers, we shuffled and stratified our data based on mobile and stationary state labels before splitting the data into training (80 %) and test (20 %) sets. This ensured that both sets preserved the class distribution of the original dataset, preventing folds from having missing classes or imbalanced proportions, which could lead to biased model evaluation. Recording sessions were generally conducted on different days, including varying stimulation levels due to active titration by both patients and clinicians. Therefore, stratification also ensured that the training and test sets had samples from various days and stimulation amplitudes. In subsequent sections, we assessed the models' performance when transferred across these different sessions and stimulation levels. For the regressors, stratification was not used because we were predicting continuous forearm speeds.

To determine the specific contributions of each feature to model performance, we calculated the permutation feature importance for each PB and brain region.[46] This process involved shuffling the sample values (10,000 permutations) to diminish the predictive power of each feature, allowing us to measure the change in model performance when

predictions were made using the altered dataset. We also computed the conditional mutual information between each PB and forearm speed measurements, as well as between PBs in each brain region and movement speeds.[47] This analysis quantified the reduction in uncertainty about forearm motion attributable to each PB and brain region, while accounting for the contribution of movement-related information from other PBs.[48,49] To examine the effects of the varying DBS current amplitudes on kinematic biomarkers, we computed movement-related Cohen's d effect sizes for each canonical power band and brain region at each stimulation level. Additionally, we explored the influence of the time interval between sessions on model performance. This was done by training models with samples from one session and testing them with data from another session at different time points. We also evaluated how stimulation amplitudes influenced our ability to decode movement by employing 5-fold stratified cross-validation to measure model performance at each stimulation level. We quantified the changes in Cohen's d values and model AUCs across different stimulation levels using LMMs.

Results

Cortical and subcortical biomarkers of naturalistic movement

We recorded intracranial signals from the somatosensory (S1) and motor (M1) cortices, as well as the subthalamic nucleus (STN; 22 hemispheres) or globus pallidus internus (GPi; 5 hemispheres) during deep brain stimulation (DBS) in patients with Parkinson's disease (Mean ± SEM duration of data collected per hemisphere: 4.2 ± 0.3 h). A total of 539 hours of data were collected, comprising 213 hours at 0 mA and 326 hours at stimulation amplitudes above 0 mA. Participants utilized wrist-worn accelerometers (Apple watches) to record their forearm speeds during unconstrained everyday activities. The timestamps of the RC+S and Apple watches were synchronized to correct for any time lags (Mean absolute time lag before correction ± standard error of the mean: 0.6 ± 0.2 s). Commencing with the raw local field potentials (LFPs), we computed flattened power spectral densities (PSDs) within 500-ms epochs. 65 % of these epochs (353 hours; 227 hours at stimulation amplitudes above 0 mA and 126 hours at 0 mA) were free from tremor or dyskinesia based on Apple watch scores. Using the local minimum of the group-level bimodal combined forearm speed distribution (28th percentile) we distinguished between mobile and stationary states.

Based on this distinction between movement states, we calculated Cohen's d (Cd) effect sizes for frequencies ranging from 0 to 100 Hz for each subject and hemisphere **(Fig. 2A)**.

Negative and positive Cd values indicated a decrease and increase in spectral power during the mobile state compared to the stationary state respectively.[50] Frequency ranges with contiguous PSDs showing negative Cd values were identified as movement-related desynchronization (MRD) bands, while those with positive Cohen's d values were identified as movement-related synchronization (MRS) bands.[12–17] For our main analyses, we opted to focus on the subset of hemispheres that were stimulated at 130 Hz (9 patients; 16 STNs and 2 GPi's), to avoid interference from varying stimulation frequencies. Additionally, analysis with all data, irrespective of stimulation frequency was also completed and included in the Supplementary material.

Shifting the speed threshold between the 5th and 95th percentiles of the combined forearm speed distribution, we computed the average Cohen's "d-gram" for each site **(Fig. 2B)**. This represented the movement-discriminative ability of each PSD (within 0 – 100 Hz) across a range of immobile/slower versus faster distributional splits. Significant MRD was observed in the alpha, low beta, and high beta ranges in cortical areas. In contrast, in the STN/GPi, high beta MRD, but not low beta MRD, reached significance at the group level (FDR-corrected, $P < 0.05$). However, on an individual level, 6 patients (9 STNs and 2 GPi's) also demonstrated significant MRD in the low beta frequency range, underscoring the variability in the predictive power of canonical PBs across participants.

Significant MRS was found in the 40 – 80 Hz range for the STN/GPi and the 60 – 100 Hz range for the S1 and M1 (FDR-corrected $P < 0.05$). These findings revealed significant predictive power from both cortical and subcortical regions albeit within site-specific frequency ranges.[12,19,50] To assess the robustness of these findings across different dopaminergic medication levels, we recreated the Cohen's d-grams within 15-minute intervals, during which variations in medication levels were likely minimal, and averaged them (FDR-corrected $P < 0.05$) **(Fig. S1A)**. We also calculated the average group-level Cohen's d-gram using the complete dataset, including periods with tremor or dyskinesia **(Fig. S1B)**. These group-level Cohen's d-grams revealed consistent alpha/beta MRD and gamma MRS bands, despite variations in medication level over time or analysis of the full recording duration.[51]

We extracted several characteristics from the MRD and MRS bands in each Cohen's d plot for comparison, including the peaks in Cohen's d (Cd_{PEAK}) and their respective frequencies (f_{PEAK}). Specifically, we determined the highest Cd value in the MRS band (MRS Cd_{PEAK}) and the most negative Cd value in the MRD band (MRD Cd_{PEAK}). There was no significant difference in the MRD Cd_{PEAK} frequencies of cortical versus subcortical sites (Median ± SEM peak frequencies; STN/GPi: 24 ± 4 Hz, S1: 22 ± 1 Hz, M1: 23 ± 1 Hz, One-way ANOVA: $F = 2.18$, $P = 0.13$) **(Fig. 2C)**. However, cortical MRS Cd_{PEAK} frequencies were higher than those in the STN/GPi (STN/GPi: 52 ± 4 Hz; S1: 64 ± 2 Hz; M1: 66 ± 2 Hz; $F = 12.16$, $P < 10^{-4}$; Post-

hoc one-sided Wilcoxon signed rank test: $W = 0.0$, $P < 0.002$). Cortical MRS Cd_{PEAK} were commonly around 65 Hz, suggesting a link between stimulation-entrained gamma power and volitional movement.[19,21]

We also compared the MRD and MRS Cd_{PEAK} magnitudes in each brain region. Cortical beta MRD Cd_{PEAK} demonstrated a greater magnitude compared to cortical gamma MRS Cd_{PEAK} ($W = 45.0$, $P = 0.003$) **(Fig. 2D)**. Additionally, cortical MRD Cd_{PEAK} ($W = 0.0$, $P = 0.002$) and MRS Cd_{PEAK} ($W = 6.0$, $P = 0.03$) exhibited higher magnitudes than those observed in the STN/GPi, indicating that cortical biomarkers were more predictive of naturalistic motion.[19,24] Moreover, we calculated the full width at half maximum of the Cohen's d values (Cd_{FWHM}) within each MRD and MRS band. The MRS Cd_{FWHM} was significantly wider than the MRD Cd_{FWHM} at each site (STN/GPi: $W = 2.0$, $P = 0.02$; S1: $W = 5.0$, $P = 0.03$; M1: $W = 8.0$, $P = 0.049$) **(Fig. 2E)**. To further examine the predictive capabilities of each brain region in estimating continuous forearm speed values, Spearman correlations between each PSD and absolute forearm speed were computed **(Fig. 2F)**. We found that alpha MRD, beta MRD and gamma MRS encoded continuous forearm speeds in each brain region (FDR-corrected $P < 0.05$). These results emphasized the presence of site-specific biomarkers associated with naturalistic motion.[8]

Movement Decoding Using Multivariate Signals and Machine Learning

Converging evidence indicates that the nervous system encodes movement-related neural activity across several frequency ranges simultaneously.[19,52] This suggests that combining neural features can potentially enhance the capacity to decode forearm movements. Therefore, we developed machine learning (ML) models with multiple features to classify stationary and mobile states or predict continuous forearm speeds during unconstrained, naturalistic motion. These models were developed using canonical PBs from an individual site (STN/GPi, S1 or M1) or by combining PB features from all three regions. Using Linear Discriminant Analysis (LDA) and 5-fold cross-validation on the training dataset, we identified the optimal epoch durations for each region by comparing the area under the receiver operating characteristic curve (AUC) scores (STN/GPi: 8 s, S1: 10 s, M1: 8 s, and Combined: 9 s) **(Fig. 3A)**. These represented the epoch durations above which there was no improvement in model performance by more than 0.01.

Significant differences in AUC between single-site and combined classifiers were observed on the holdout dataset ($F = 5.35$, $P = 0.004$) **(Fig. 3B)**. The combined classifier had the highest performance (Mean ± SEM AUC: 0.84 ± 0.01; $W > 42.0$, $P < 0.002$).[22] Cortical sites were more predictive of movement states compared to the STN/GPi ($W > 40.0$, $P < 0.03$) although there was no significant difference in performance between the S1 and M1 models ($W = 24.0$, $P = 0.46$).[53,54] To provide a comprehensive assessment of our models, we

also computed several other metrics, such as balanced accuracy, F1 score, sensitivity, specificity and positive predictive value, **(Table 2)**.

Prior studies have demonstrated that customizing features for individual patients can enhance the performance of predictive models.[22,28] Consequently, besides using canonical power bands, we employed principal component analysis (PCA) and identified the number of PC features for optimal classifier performance (STN/GPi: 8, S1: 4, M1: 5, Combined: 6) **(Fig. 3C)**. We also computed the cumulative explained variance of these PCs (Mean ± SEM variance: STN/GPi: 81 ± 2 %, S1: 59 ± 2 %, M1: 65 ± 2 %, Combined: 47 ± 2 %) **(Fig. S2A)** and the PC loadings of the first PC (FDR-corrected $P < 0.05$) **(Fig. S2B)**. Like with canonical PBs, the combined classifiers yielded the highest AUC (Mean ± SEM AUC: 0.83 ± 0.01; $F = 3.89$, $P = 0.02$; $W = 45.0$, $P = 0.002$) **(Fig. 3D)**. We found no significant difference between linear models using personalized PCs and those using canonical PBs ($W = 20.0$, $P = 0.63$). This was likely due to the use of 6 canonical PB features per site. However, real-world devices may impose additional model restrictions (e.g. maximum 4 PBs for the Summit RC+S) which may lead to improved performance through personalization of features.[24]

We determined the permutation feature importance of each site to quantify their specific contributions to movement decoding (Mean ± SEM change in AUC; STN/GPi: -0.05 ± 0.01, S1: -0.12 ± 0.02, M1: -0.10 ± 0.02; $W = 0.0$, $P = 0.004$) **(Fig. 3E)**. The contribution from the S1 was greater than that from the STN/GPi ($W = 41.0$, $P = 0.041$) but similar to that from the M1 ($W = 19.0$, $P = 0.37$). These findings suggested that the basal ganglia and sensorimotor cortex encode distinct, non-redundant movement-related information.[7,8,54] We examined the permutation feature importance of individual PBs in each brain region. Among these, cortical high beta power demonstrated the highest feature importance (Mean ± SEM change in AUC: -0.10 ± 0.02), indicating that it was the most predictive biomarker of naturalistic movement amongst the PBs ($F = 2.74$, $P = 0.0005$; $W = 6.0$, $P = 0.027$) **(Fig. 3F)**.[14]

Although simple linear classifiers can be embedded on current implantable neurostimulators, more advanced models may yield higher performance for real-time movement decoding.[23] Therefore, we evaluated the effectiveness of more complex models, including k-nearest neighbor (kNN), random forest (RF), and light gradient-boosting machine (LGBM) **(Fig. 3G)**. We also included all 50 PSDs from each site as features for these non-linear models, rather than restricting them to the canonical PB features. The RF classifier achieved a small but significant improvement over linear models that used PB features (Mean ± SEM AUC: 0.85 ± 0.01), with a difference in AUC of 0.016 ± 0.004 ($F = 3.25$, $P = 0.01$; $W = 0$, $P = 0.007$). These findings suggested that while canonical power bands were effective as kinematic biomarkers, employing complex classifiers could offer a slight enhancement in movement prediction.[19]

In addition to assessing binary movement states, we aimed to evaluate the utility of the multivariate signals in predicting absolute forearm speeds. To achieve this, we repeated our classifier analysis on linear regression models using canonical PBs from one or all sites and obtained similar results. Using Pearson's correlations between predicted and actual speeds (*r* statistic) as the primary metric, we determined the optimal epoch duration for each model (STN/GPi: 10 s, S1: 10 s, M1: 11 s, Combined: 10 s) **(Fig. 4A)**. Combining cortico-basal signals yielded the highest-performing models (Mean *r* statistic ± SEM: 0.64 ± 0.03; $F = 6.35$, $P = 0.002$; $W = 45.0$, $P = 0.002$) **(Fig. 4B).** We also explored the use of personalized PCs as features. We identified the optimal number of PCs for each model (STN/GPi: 9, S1: 5, M1: 8, Combined: 8) **(Fig. 4C)** and found that integrating PC features from all sites improved model performance (Mean *r* statistic ± SEM: 0.63 ± 0.03; $F = 4.69$, $P = 0.008$; $W = 45.0$, $P = 0.003$) **(Fig. 4D)**, reinforcing the hypothesis that each site encodes distinct movement-related information.[52]

To assess the marginal movement decoding ability of each brain region, we calculated their respective permutation feature importance. Each site made significant, unique contributions to movement prediction ($W = 0.0$, $P = 0.004$) although the S1 had higher feature importance than the STN/GPi ($W = 44.0$, $P = 0.01$) **(Fig. 4E)**. Cortical high beta power had the highest feature importance (Mean ± SEM change in *r* statistic: -0.19 ± 0.03) compared to other PBs, including cortical low beta ($W = 2.0$, $P = 0.006$) **(Fig. 4F)**. This suggested significant differences between low and high cortical beta power in decoding forearm speed.[14]

As an additional measure of feature importance, we computed the conditional mutual information for each PB and brain region.[47–49] Specifically, we calculated the marginal mutual information between each PB feature and forearm speed measurements, conditioned on the other cortical and subcortical PBs **(Fig. S5A)**. We also assessed the joint mutual information between PBs in each brain region and movement speeds, conditioned on PBs from other brain regions **(Fig. S5B)**. The conditional mutual information from the S1 was greater than that from the STN/GPi ($W = 3.0$, $P = 0.029$) but not significantly different from the M1 ($W = 38.0$, $P = 0.056$). Additionally, we found that cortical high beta power had the highest conditional mutual information (Mean ± SEM MI: 0.020 ± 0.003). These findings corroborated our findings that the basal ganglia and sensorimotor cortex encode distinct, non-redundant movement-related information and that cortical high beta was the most predictive biomarker of naturalistic movement amongst the PBs ($F = 2.67$, $P = 8.1 \times 10^{-4}$; $W = 2.0$, $P = 0.002$).

Due to the high multicollinearity among spectral features, canonical PBs were used for non-linear regression models (kNN, RF and LGBM). There was no significant variability in

performance amongst the models ($F = 0.28$, $P = 0.92$) **(Fig. 4G)**. However, post-hoc analysis revealed that the LGBM (Mean ± SEM r statistic: 0.69 ± 0.03) and RF (Mean ± SEM r statistic: 0.68 ± 0.03) regressors achieved significantly higher performance than the linear PB-based model ($W > 1.0$, $P < 0.033$). This further validated our finding that complex non-linear models could slightly improve model performance.[19,23] For completeness, we re-ran our machine learning pipeline on the full patient cohort, including those with stimulation frequencies different from 130 Hz, and obtained similar results **(Table S1)** for both the classifiers **(Figs. S3A-D)** and regressors **(Figs. S4A-D**).

Effects of stimulation current amplitude on movement decoding

Previous studies have demonstrated that DBS can influence neural signals, such as reducing resting-state subcortical beta activity in patients with Parkinson's disease.[12,20,55] However, the effects of varying stimulation levels on kinematic biomarkers and movement-predictive ML models have not previously been evaluated. Understanding this impact can also provide insights into the potential performance of movement-responsive BCI-aDBS systems, which decode neural signals in real-time at different stimulation current amplitudes.[26,56] To address this gap, we investigated the effects of stimulation levels on movement-related changes in alpha, beta, and gamma PBs. An example of movement-related changes in STN spectral power for a single subject when DBS was at 0.0 mA or 2.0 mA is shown in **Figs. 5A & 5B**.

Absolute Cohen's d effect sizes were used to quantify the movement-related desynchronization/synchronization of canonical PBs in each brain region. To evaluate the relationship between these effect sizes and stimulation amplitudes, we employed linear mixed models (LMMs) with stimulation amplitude modeled as a fixed effect, while individual patients and hemispheres were included as random effects. To visualize these relationships, we plotted the average absolute Cd values at each stimulation amplitude across all patients for the STN/GPi **(Fig. 5C)**, S1 **(Fig. 5D)** and M1 **(Fig. 5E)**. Increasing the stimulation amplitude was correlated with a decrease in the MRD of subcortical low beta (STN/GPi: $\beta = -0.078$; 95 % CI = [-0.1221, -0.036], $P = 0.003$), high beta (STN/GPi: $\beta = -0.103$; 95 % CI = [-0.145, -0.060], $P < 10^{-4}$) and low gamma (STN/GPi: $\beta = -0.050$; 95 % CI = [-0.083, -0.018], $P = 0.006$), as evidenced by a reduction in absolute Cd values. In contrast, cortical regions showed no significant effect on high beta MRD. There was, however, a stimulation-related decrease in alpha MRD (S1: $\beta = -0.034$; 95 % CI = [-0.061, -0.007], $P = 0.045$) (M1: $\beta = -0.035$; 95 % CI = [-0.061, -0.008], $P = 0.02$) and low beta MRD (S1: $\beta = -0.048$; 95 % CI = [-0.085, -0.010], $P = 0.045$) (M1: $\beta = -0.072$; 95 % CI = [-0.118, -0.026], $P = 0.009$), as well as an increase in M1 stimulation-entrained gamma MRS (M1: $\beta = 0.044$; 95 % CI = [0.018,

0.069], $P = 0.006$). This revealed that stimulation levels affected site-specific biomarkers of naturalistic motion.

To examine how the time interval between recording sessions affected the performance of movement-predictive classifiers, we trained the ML models on data from one session and tested them on data from subsequent sessions conducted at the same stimulation amplitude. We incorporated the duration between sessions as a fixed effect in our LMMs, while treating individual patients and hemispheres as random effects (**Fig. 5F**). Further, we explored the impact of stimulation levels on classifier performance by performing 5-fold cross-validation on data collected from each session **(Fig. 5G)**. We incorporated the stimulation level as a fixed effect in our LMMs, with individual patients and hemispheres treated as random effects. We then repeated this analysis to assess the effects of duration between recording sessions **(Fig. 5H)** and stimulation amplitude **(Fig. 5I)** on regressor performance. The performance of both the classifiers and regressors maintained stability over time (Max duration: 83 days; Median ± SEM duration: 6 ± 2 days) ($\beta < 0.033$, $P > 0.34$). STN/GPi classifiers ($\beta = -0.030$; 95 % CI = [-0.046, -0.013], $P = 0.004$) and regressors ($\beta = -0.054$; 95 % CI = [-0.086, -0.023], $P = 0.004$) demonstrated lower performance at higher stimulation amplitudes. Conversely, the S1, M1, and combined models were not significantly affected by changes in stimulation levels ($\beta > -0.019$, $P > 0.05$). This was likely due to the preserved predictive power of cortical high beta MRD at higher stimulation amplitudes.

Discussion

We identified cortico-basal biomarkers of naturalistic forearm movement by analyzing over 530 hours of neural and accelerometry recordings from 15 patients with Parkinson's disease during deep brain stimulation (DBS).[21,44] Specifically, we observed beta movement-related desynchronization (MRD) and gamma movement-related synchronization (MRS) in both cortical and subcortical regions.[13,50,51,57] Although we did not specifically track the medication timings of our patient cohort, we repeated our biomarker analyses within 15-minute windows, during which medication states were likely stable. This approach demonstrated that these biomarkers remained predictive of movement across different medication states, rather than merely decoding slow medication state fluctuations. Using a multivariate machine learning (ML) approach, we revealed distinct contributions from each brain region in predicting movement, with cortical high beta MRD being the most discriminative signal.[52,58] Consequently, ML models that incorporated both cortical and subcortical signals demonstrated superior model performance compared to single-site

models. We also found that DBS amplitudes influenced the performance of these models, with higher stimulation levels leading to a decrease in the accuracy of subcortical models.[26,55] Despite this, cortical and combined cortico-basal models continued to perform well at higher stimulation levels. This sustained performance supports the future potential of movement responsive BCI-aDBS.[23,24]

Subcortical low and high beta power encode distinct movement-related functions

Within the beta frequency range (12 – 30 Hz), we revealed group-level functional distinctions between low (12 – 20 Hz) and high (20 – 30 Hz) subcortical beta rhythms, which have both previously been associated with motor execution.[13] Higher Parkinson's disease-related bradykinesia severity has also been correlated with increased low beta power.[12] Treatments, such as dopaminergic medication and DBS, have been found to suppress low beta activity and reduce bradykinesia severity.[58,59] In contrast, high beta has been linked to physiological mechanisms, such as force generation and voluntary motor actions.[60] This suggests that low beta may be functionally 'anti-kinetic' in the pathophysiology of Parkinson's disease, whereas high beta might have a stronger association with the execution of normal motor plans.[14] Our study supports this difference in physiological roles by demonstrating that MRD associated with naturalistic movement, irrespective of dopaminergic state, was only observed within the high beta band.

Cortical stimulation-entrained gamma is associated with naturalistic movement

Cortical and subcortical broadband gamma MRS has been linked to motor speed and complexity in both healthy individuals and patients with Parkinson's disease.[50,57] During DBS, cortical and subcortical oscillations at subharmonics of the stimulation frequency have also been observed.[21] Specifically, entrainment at the half-harmonic (~65 Hz) of the 130 Hz stimulation frequency have been noted.[61] Broadband gamma activity is non-oscillatory and thought to represent asynchronous neuronal spiking activity across a wide frequency range (30 – 200 Hz).[62] In contrast, recent studies have shown that stimulation-entrained gamma oscillations are associated with synchronized spiking and are influenced by dopaminergic medication and sleep-wake cycles, indicating a non-artefactual, physiological role for these neural signals.[30,31] Consistent with these findings, we detected broadband gamma movement-related synchronization within the cortical regions. In our cohort of patients stimulated at 130 Hz, stimulation-entrained gamma MRS at ~65 Hz was significantly greater than that at the other frequencies within the broadband gamma range.[63] This suggests that entrained gamma power more effectively distinguishes between

movement states than broadband gamma and may serve as a valuable, kinematic biomarker in the ON-stimulation state.[64]

Subcortical and cortical sites provide complementary information for movement decoding

The sensorimotor cortex is involved in motor planning and execution while the basal ganglia plays a more implicit, regulatory role in selecting and initiating movements, inhibiting unwanted actions, and refining motor skill.[2,4,8,9] Furthermore, prior research by our group revealed that combining spectral features from cortical and subcortical regions can improve the accuracy of linear models in decoding Parkinson's disease-related symptom states, such as severe bradykinesia or dyskinesia.[22] These findings suggest that cortical and subcortical signals encode specific information regarding naturalistic motion. Consistent with these findings, this study demonstrates that integrating subcortical and cortical signals yielded more accurate ML models for predicting movement than using signals from individual sites alone indicating complementary encoding. Feature importance analyses further confirmed the significant contributions of each brain region to the performance of the combined models. Repeating our analysis on the full patient cohort, we observed similar model performance and feature importance across different stimulation frequencies (other than 130 Hz).

DBS modulates movement-related cortico-basal biomarkers

Movement-related changes in the spectral power of cortical and subcortical biomarkers were influenced by DBS amplitudes. Specifically, increased stimulation levels were found to correlate with lower subcortical beta MRD and gamma MRS, as evidenced by a reduction in absolute Cohen's d effect size.[26] This reduction potentially impacted the discriminative power of beta and gamma biomarkers at higher stimulation levels, thus decreasing the accuracy of subcortical models for movement prediction. In the sensorimotor cortex, higher DBS levels were associated with reduced low beta MRD, suggesting that patients could achieve similar movement speeds with decreased beta MRD. This aligns with previous findings showing higher cortical beta MRD in Parkinson's disease patients than individuals with essential tremor or without movement disorders.[17,65] Moreover, dopaminergic medication is associated with a reduction in cortical beta MRD and an improvement in motor speed.[51] In contrast to our subcortical models, those using cortical signals or integrating cortico-basal signals demonstrated greater stability. This was likely due to the resilience of cortical high beta MRD, identified as the most discriminative kinematic biomarker. Therefore, integrating cortico-basal signals could enhance the

accuracy and stability of movement prediction across varying stimulation conditions, which is crucial for the development of BCI-aDBS systems to treat motor disorders.

Implications for closed-loop DBS treatments

Based on the gating theory of basal ganglia function, the basal ganglia excessively inhibits the initiation and execution of motor plans, exacerbating these hypokinetic symptoms.[25] By increasing stimulation amplitudes during movement, we may be able to disinhibit the execution of these movements only when it is most needed and alleviate bradykinesia severity.[24] However, ensuring the therapeutic efficacy of a movement-based adaptive DBS policy requires careful optimization of both upper and lower stimulation levels. The upper stimulation levels must be constrained to prevent excessive stimulation, which can lead to side effects such as dyskinesia, particularly during medication-ON periods. Similarly, the lower stimulation levels should not be set too low during rest periods to avoid breakthrough tremor, especially during medication-OFF periods.

To be deployable for everyday use, such an adaptive DBS paradigm must be able to accurately decode unconstrained, volitional motion from neural signals. However, previous studies have primarily focused on decoding movement during short, constrained tasks, such as finger-tapping and hand rotations. Our study is the first to demonstrate the accurate prediction of unsupervised, naturalistic movements using chronic neural recordings during DBS. (classifier AUC > 0.85 and regressor r statistic > 0.68). We also highlight the importance of recording neural signals from both cortical regions and the basal ganglia, as integrating these signals may improve the performance and stability of movement-predictive models. With these findings, we support the development of an integrated BCI-aDBS approach that combines the fast and precise motor-decoding capabilities of emerging BCIs with the therapeutic neuromodulatory effects of aDBS.

Conclusions

Our findings demonstrate the complimentary contributions of cortico-basal neural circuits and signals in naturalistic, unconstrained, movements. We identified multivariate movement encoding particularly through cortico-basal beta and gamma oscillations, as well as stimulation-entrained gamma, in the presence of DBS. We developed ML techniques for fast and accurate decoding of unconstrained movement and identified features which were resilient to changes in stimulation conditions. This validates the potential feasibility of BCI-aDBS in naturalistic settings and opens a translational pipeline for precise motor network re-tuning in disorders of movement, including Parkinson's disease and stroke.

Data availability

De-identified, processed neural and accelerometry data can be provided upon request according to the data-sharing policies of the National Institutes of Health (NIH).

Acknowledgements

We thank our patient cohort for their involvement in this study. We also gratefully acknowledge Medtronic, Inc. for providing the Summit RC+S devices used in this study at no cost.

Funding

Grant number: UH3NS100544, Funding body: National Institutes of Health; Grant number: R01NS090913. Funding body: National Institutes of Health; Grant number: U24NS113637-01. Funding body: National Institutes of Health.

Competing interests

P.A.S. receives funding from Medtronic, Inc. and Boston Scientific Inc. for salary support of clinical fellows. P.A.S is a consultant for INBRAIN Neuroelectronics Inc. SJL is a consultant for Iota Biosciences. PAS, SJL and DL are listed inventors on the patent US2024/041516 which relates to daytime decoding of movement for BCI-aDBS in neurological disorders, including Parkinson's disease and stroke.

Supplementary material

Supplementary material is available at *Brain* online.

References

1. Bouton CE, Shaikhouni A, Annetta N V., et al. Restoring cortical control of functional movement in a human with quadriplegia. *Nature*. 2016;533:247-250. doi:10.1038/nature17435

2. McGregor MM, Nelson AB. Circuit Mechanisms of Parkinson's Disease. *Neuron*. 2019;101(6):1042-1056. doi:10.1016/j.neuron.2019.03.004

3. Cacciola A, Calamuneri A, Milardi D, et al. A connectomic analysis of the human basal ganglia network. *Front Neuroanat*. 2017;11. doi:10.3389/fnana.2017.00085

4. Nambu A, Tokuno H, Takada M. *Functional Significance of the CorticoÁ/ SubthalamoÁ/ Pallidal "hyperdirect" Pathway*. www.elsevier.com/locate/neures

5. Forstmann BU, Keuken MC, Jahfari S, et al. Cortico-subthalamic white matter tract strength predicts interindividual efficacy in stopping a motor response. *Neuroimage*. 2012;60(1):370-375. doi:10.1016/j.neuroimage.2011.12.044

6. Neumann WJ, Jha A, Bock A, et al. Cortico-pallidal oscillatory connectivity in patients with dystonia. *Brain*. 2015;138(7):1894-1906. doi:10.1093/brain/awv109

7. Park J, Phillips JW, Guo JZ, Martin KA, Hantman AW, Dudman JT. Motor cortical output for skilled forelimb movement is selectively distributed across projection neuron classes. *Sci Adv*. 2022;8(10):5167. doi:10.1126/sciadv.abj5167

8. Hansen JY, Cauzzo S, Singh K, et al. Integrating brainstem and cortical functional architectures. *Nat Neurosci*. 2024;27(12):2500-2511. doi:10.1038/s41593-024-01787-0

9. Parent A, Hazrati LN. *Full-Length Review Functional Anatomy of the Basal Ganglia. II. The Place of Subthalamic Nucleus and External Pallidum in Basal Ganglia Circuitry*.; 1995.

10. Friedman AD, Yin HH. Selective activation of subthalamic nucleus output quantitatively scales movements. *Journal of Neuroscience*. 2023;43(47):7967-7981. doi:10.1523/JNEUROSCI.0734-23.2023

11. Kühn AA, Kupsch A, Schneider GH, Brown P. Reduction in subthalamic 8-35 Hz oscillatory activity correlates with clinical improvement in Parkinson's disease.

European Journal of Neuroscience. 2006;23(7):1956-1960. doi:10.1111/j.1460-9568.2006.04717.x

12. Mathiopoulou V, Lofredi R, Feldmann LK, et al. Modulation of subthalamic beta oscillations by movement, dopamine, and deep brain stimulation in Parkinson's disease. *NPJ Parkinsons Dis*. 2024;10(1). doi:10.1038/s41531-024-00693-3

13. Kühn AA, Williams D, Kupsch A, et al. Event-related beta desynchronization in human subthalamic nucleus correlates with motor performance. *Brain*. 2004;127(4):735-746. doi:10.1093/brain/awh106

14. Torrecillos F, He S, Kühn AA, Tan H. Average power and burst analysis revealed complementary information on drug-related changes of motor performance in Parkinson's disease. *NPJ Parkinsons Dis*. 2023;9(1). doi:10.1038/s41531-023-00540-x

15. Fischer P, Pogosyan A, Herz DM, et al. Subthalamic nucleus gamma activity increases not only during movement but also during movement inhibition. *Elife*. 2017;6. doi:10.7554/eLife.23947

16. Fischer P, Pogosyan A, Cheeran B, et al. Subthalamic nucleus beta and gamma activity is modulated depending on the level of imagined grip force. *Exp Neurol*. 2017;293:53-61. doi:10.1016/j.expneurol.2017.03.015

17. Rowland NC, De Hemptinne C, Swann NC, et al. Task-related activity in sensorimotor cortex in Parkinson's disease and essential tremor: Changes in beta and gamma bands. *Front Hum Neurosci*. 2015;9(September). doi:10.3389/fnhum.2015.00512

18. Volkova K, Lebedev MA, Kaplan A, Ossadtchi A. Decoding Movement From Electrocorticographic Activity: A Review. *Front Neuroinform*.*Frontiers Media S.A*. 2019;13. doi:10.3389/fninf.2019.00074

19. Merk T, Peterson V, Lipski WJ, et al. Electrocorticography is superior to subthalamic local field potentials for movement decoding in Parkinson's disease. *Elife*. 2022;11. doi:10.7554/eLife.75126

20. Little S, Brown P. *Parkinsonism and Related Disorders 20S1 (2014) S44-S48 The Functional Role of Beta Oscillations in Parkinson's Disease*.; 2013.

21. Oehrn CR, Cernera S, Hammer LH, et al. Chronic adaptive deep brain stimulation versus conventional stimulation in Parkinson's disease: a blinded randomized feasibility trial. *Nat Med*. Published online November 1, 2024. doi:10.1038/s41591-024-03196-z

22. Gilron R, Little S, Perrone R, et al. Long-term wireless streaming of neural recordings for circuit discovery and adaptive stimulation in individuals with Parkinson's disease. *Nat Biotechnol*. 2021;39(9):1078-1085. doi:10.1038/s41587-021-00897-5

23. Dong Y, Wang S, Huang Q, Berg RW, Li G, He J. Neural Decoding for Intracortical Brain-Computer Interfaces. *Cyborg and Bionic Systems*. 2023;4. doi:10.34133/cbsystems.0044

24. Dixon TC, Strandquist G, Zeng A, et al. Movement-responsive deep brain stimulation for Parkinson's disease using a remotely optimized neural decoder. *Nat Biomed Eng*. Published online June 27, 2025. doi:10.1038/s41551-025-01438-0

25. Darbin O, Hatanaka N, Takara S, et al. Subthalamic nucleus deep brain stimulation driven by primary motor cortex γ2 activity in parkinsonian monkeys. *Sci Rep*. 2022;12(1). doi:10.1038/s41598-022-10130-1

26. He S, Baig F, Merla A, et al. Beta-triggered adaptive deep brain stimulation during reaching movement in Parkinson's disease. *Brain*. 2023;146(12):5015-5030. doi:10.1093/brain/awad233

27. Cernera S, Alcantara JD, Opri E, et al. Wearable sensor-driven responsive deep brain stimulation for essential tremor. *Brain Stimul*. 2021;14(6):1434-1443. doi:10.1016/j.brs.2021.09.002

28. Opri E, Cernera S, Molina R, et al. *Chronic Embedded Cortico-Thalamic Closed-Loop Deep Brain Stimulation for the Treatment of Essential Tremor*. Vol 12.; 2020. https://www.science.org

29. Follett KA, Weaver FM, Stern M, et al. Pallidal versus Subthalamic Deep-Brain Stimulation for Parkinson's Disease. *New England Journal of Medicine*. 2010;362(22):2077-2091. doi:10.1056/nejmoa0907083

30. Sermon JJ, Olaru M, Ansó J, et al. Sub-harmonic entrainment of cortical gamma oscillations to deep brain stimulation in Parkinson's disease: Model based predictions and validation in three human subjects. *Brain Stimul*. 2023;16(5):1412-1424. doi:10.1016/j.brs.2023.08.026

31. Olaru M, Hahn A, Shcherbakova M, et al. Deep brain stimulation-entrained gamma oscillations in chronic home recordings in Parkinson's disease. *Brain Stimul*. 2025;18(2):132-141. doi:10.1016/j.brs.2025.01.011

32. Sellers KK, Gilron R, Anso J, et al. Analysis-rcs-data: Open-Source Toolbox for the Ingestion, Time-Alignment, and Visualization of Sense and Stimulation Data From

the Medtronic Summit RC+S System. *Front Hum Neurosci*. 2021;15. doi:10.3389/fnhum.2021.714256

33. Neumann WJ, Memarian Sorkhabi M, Benjaber M, et al. The sensitivity of ECG contamination to surgical implantation site in brain computer interfaces. *Brain Stimul*. 2021;14(5):1301-1306. doi:10.1016/j.brs.2021.08.016

34. Hammer LH, Kochanski RB, Starr PA, Little S. Artifact Characterization and a Multipurpose Template-Based Offline Removal Solution for a Sensing-Enabled Deep Brain Stimulation Device. *Stereotact Funct Neurosurg*. 2022;100(3):168-183. doi:10.1159/000521431

35. Powers R, Etezadi-Amoli M, Arnold EM, et al. *Smartwatch Inertial Sensors Continuously Monitor Real-World Motor Fluctuations in Parkinson's Disease*. Vol 13.; 2021. https://www.science.org

36. Benjamini Y, Yekutieli D. *THE CONTROL OF THE FALSE DISCOVERY RATE IN MULTIPLE TESTING UNDER DEPENDENCY*. Vol 29.; 2001.

37. McKeown DJ, Finley AJ, Kelley NJ, et al. Test-retest reliability of spectral parameterization by 1/f characterization using SpecParam. *Cerebral Cortex*. 2024;34(1). doi:10.1093/cercor/bhad482

38. Donoghue T, Haller M, Peterson EJ, et al. Parameterizing neural power spectra into periodic and aperiodic components. *Nat Neurosci*. 2020;23(12):1655-1665. doi:10.1038/s41593-020-00744-x

39. Anjum MF, Smyth C, Zuzuárregui R, et al. Multi-night cortico-basal recordings reveal mechanisms of NREM slow-wave suppression and spontaneous awakenings in Parkinson's disease. *Nat Commun*. 2024;15(1). doi:10.1038/s41467-024-46002-7

40. Lakens D. Calculating and reporting effect sizes to facilitate cumulative science: a practical primer for t-tests and ANOVAs. *Front Psychol*. 2013;4. doi:10.3389/fpsyg.2013.00863

41. Huang J, Ling CX. *Using AUC and Accuracy in Evaluating Learning Algorithms*. http://www.computer.org/publications/dlib

42. Richardson E, Trevizani R, Greenbaum JA, Carter H, Nielsen M, Peters B. The receiver operating characteristic curve accurately assesses imbalanced datasets. *Patterns*. 2024;5(6). doi:10.1016/j.patter.2024.100994

43. Chawla N V, Bowyer KW, Hall LO, Kegelmeyer WP. *SMOTE: Synthetic Minority Over-Sampling Technique*. Vol 16.; 2002.

44. Olaru M, Cernera S, Hahn A, et al. Motor network gamma oscillations in chronic home recordings predict dyskinesia in Parkinson's disease. *Brain*. 2024;147(6):2038-2052. doi:10.1093/brain/awae004

45. Das K, Jiang J, Rao JNK. Mean squared error of empirical predictor. *The Annals of Statistics*. 2004;32(2):818-840. doi:10.1214/009053604000000201

46. Altmann A, Toloşi L, Sander O, Lengauer T. Permutation importance: A corrected feature importance measure. *Bioinformatics*. 2010;26(10):1340-1347. doi:10.1093/bioinformatics/btq134

47. Fleuret F. *Fast Binary Feature Selection with Conditional Mutual Information*. Vol 5.; 2004. http://diwww.epfl.ch/

48. Zhang Y, Zhang Z. Feature subset selection with cumulate conditional mutual information minimization. *Expert Syst Appl*. 2012;39(5):6078-6088. doi:10.1016/j.eswa.2011.12.003

49. Souza F, Premebida C, Araújo R. High-order conditional mutual information maximization for dealing with high-order dependencies in feature selection. *Pattern Recognit*. 2022;131. doi:10.1016/j.patcog.2022.108895

50. Crone NE, Miglioretti DL, Gordon B, Lesser RP. *Functional Mapping of Human Sensorimotor Cortex with Electrocorticographic Spectral Analysis II. Event-Related Synchronization in the Gamma Band*. Vol 121.; 1998.

51. Chung JW, Burciu RG, Ofori E, et al. Beta-band oscillations in the supplementary motor cortex are modulated by levodopa and associated with functional activity in the basal ganglia. *Neuroimage Clin*. 2018;19:559-571. doi:10.1016/j.nicl.2018.05.021

52. Peterson V, Merk T, Bush A, et al. Movement decoding using spatio-spectral features of cortical and subcortical local field potentials. *Exp Neurol*. 2023;359. doi:10.1016/j.expneurol.2022.114261

53. Lauro PM, Lee S, Amaya DE, Liu DD, Akbar U, Asaad WF. Concurrent decoding of distinct neurophysiological fingerprints of tremor and bradykinesia in Parkinson's disease. *Elife*. 2023;12. doi:10.7554/eLife.84135

54. Todorov D, Schnitzler A, Hirschmann J. Parkinsonian rest tremor can be distinguished from voluntary hand movements based on subthalamic and cortical activity. *Clinical Neurophysiology*. 2024;157:146-155. doi:10.1016/j.clinph.2023.10.018

55. Chen Y, Gong C, Tian Y, et al. Neuromodulation effects of deep brain stimulation on beta rhythm: A longitudinal local field potential study. *Brain Stimul*. 2020;13(6):1784-1792. doi:10.1016/j.brs.2020.09.027

56. Little S, Pogosyan A, Neal S, et al. Adaptive deep brain stimulation in advanced Parkinson disease. *Ann Neurol*. 2013;74(3):449-457. doi:10.1002/ana.23951

57. Lofredi R, Neumann WJ, Bock A, et al. Dopamine-dependent scaling of subthalamic gamma bursts with movement velocity in patients with Parkinson's disease. *Elife*. 2018;7. doi:10.7554/eLife.31895

58. Oswal A, Beudel M, Zrinzo L, et al. Deep brain stimulation modulates synchrony within spatially and spectrally distinct resting state networks in Parkinson's disease. *Brain*. 2016;139(5):1482-1496. doi:10.1093/brain/aww048

59. Lofredi R, Okudzhava L, Irmen F, et al. Subthalamic beta bursts correlate with dopamine-dependent motor symptoms in 106 Parkinson's patients. *NPJ Parkinsons Dis*. 2023;9(1). doi:10.1038/s41531-022-00443-3

60. Florin E, Dafsari HS, Reck C, et al. Modulation of local field potential power of the subthalamic nucleus during isometric force generation in patients with Parkinson's disease. *Neuroscience*. 2013;240:106-116. doi:10.1016/j.neuroscience.2013.02.043

61. Swann NC, De Hemptinne C, Miocinovic S, et al. Gamma oscillations in the hyperkinetic state detected with chronic human brain recordings in parkinson's disease. *Journal of Neuroscience*. 2016;36(24):6445-6458. doi:10.1523/JNEUROSCI.1128-16.2016

62. Manning JR, Jacobs J, Fried I, Kahana MJ. Broadband shifts in local field potential power spectra are correlated with single-neuron spiking in humans. *Journal of Neuroscience*. 2009;29(43):13613-13620. doi:10.1523/JNEUROSCI.2041-09.2009

63. Amengual JL, Vernet M, Adam C, Valero-Cabré A. Local entrainment of oscillatory activity induced by direct brain stimulation in humans. *Sci Rep*. 2017;7. doi:10.1038/srep41908

64. Mathiopoulou V, Habets J, Feldmann LK, et al. DBS-induced gamma entrainment as a new biomarker for motor improvement with neuromodulation. Preprint posted online April 26, 2024. doi:10.1101/2024.04.25.24306357

65. Kondylis ED, Randazzo MJ, Alhourani A, et al. Movement-related dynamics of cortical oscillations in Parkinson's disease and essential tremor. *Brain*. 2016;139(8):2211-2223. doi:10.1093/brain/aww144

66. Khawaldeh S, Tinkhauser G, Shah SA, et al. Subthalamic nucleus activity dynamics and limb movement prediction in Parkinson's disease. *Brain*. 2020;143(2):582-586. doi:10.1093/brain/awz417

Figure legends

Figure 1 Anatomic localization of implanted electrodes and single-subject example of processed neural and accelerometry data. (A) Schematic of patient performing activity of daily living while streaming data from implanted neurostimulators and wrist-worn accelerometers. (B) Cortical electrodes represented on a template brain. Five of the fifteen patients in our cohort used an overlapping sensing configuration (Electrode pairs: 1-3 and 2-4). The remaining ten subjects used a non-overlapping configuration (Electrode pairs: 1-2 and 3-4). (C) Subcortical electrodes represented on a template brain in the globus pallidus externus (GPe), globus pallidus internus (GPi), subthalamic nucleus (STN) and red nucleus (RN). (D) Neural and accelerometry data processing pipeline. (E) Single-subject (Pat-01) spectrograms based on data streamed from the left STN, primary somatosensory cortex (S1) and primary motor cortex (M1). Right forearm speeds were recorded simultaneously. (F) Single-subject average power spectral densities (PSDs) were computed from the STN, S1 and M1 signals and fitted with the Spectral Parameterization algorithm to compare between mobile and stationary states. (G) The corresponding flattened PSD plots have been displayed. The beta band (12 – 30 Hz) has been highlighted in green. (H) Forearm speeds from all patients in our cohort were combined and displayed in a kernel density estimate plot. A local minimum was identified at the 28th percentile of the distribution (termed the movement state threshold) and used to distinguish between mobile and stationary states. (I) Cohen's d (Cd) effect sizes based on the flattened PSDs from a single subject were calculated and used to create a Cd plot. These values quantified the differences in spectral power between movement states. The frequencies with positive Cd values, indicating an increase in spectral power during mobile states compared to stationary states, were highlighted in red. Several characteristics, such as the peak frequency (f_{PEAK}), maximum Cohen's d (Cd_{PEAK}) and full width at half maximum (Cd_{FWHM}), were extracted from this band. The frequencies with negative Cd values were highlighted in blue.

Figure 2 Cortical and subcortical biomarkers of naturalistic movement. (A) Cohen's d (Cd) plots for each patient and hemisphere were computed using STN/GPi (left), S1 (middle) and M1 (right) signals. Four out of fifteen patients in our cohort had a different stimulation frequency than 130 Hz and two of were recording while stimulation was OFF (marked by asterisks). The largest frequency range with contiguous positive Cd values (highlighted in red) was termed the movement-related synchronization (MRS) band while that with contiguous negative Cd values (highlighted in blue) was termed the movement-related desynchronization (MRD) band. In cases where a hemisphere exhibited multiple MRD or MRS bands, the band with the highest average absolute Cd value was selected for further analysis. (B) Each percentile (between the 5th and 95th percentiles) of the group-level forearm speed distribution (from Fig. 1H) was used as a threshold to produce one-dimensional Cd plots discriminating slower from faster movements. These plots were concatenated to create two-dimensional Cohen's "d-grams" (Cd-grams). The horizontal dotted line in each Cd-gram lies on the 28th percentile which distinguishes between mobile and stationary states. The grey masks indicate the regions that did not survive false discovery rate (FDR) correction ($P \geq 0.05$). (C) Using the 28th percentile threshold, we identified the frequencies with the lowest (most negative) and highest (most positive) Cd values from each hemisphere. These were termed the MRD and MRS Cd_{PEAK} frequencies respectively. Additionally, we calculated (D) the absolute Cd_{PEAK} magnitudes and (E) the full widths at half maximum (Cd_{FWHM}) of the MRD and MRS bands (based on the Cd plots in Fig. 2A). (F) FDR-corrected average Spearman correlation (ρ) values between the PSDs and the absolute forearm speeds were computed. The resulting significant frequency bands have been highlighted by the color-coded bars above the respective plots. *$P \leq 0.05$, **$P \leq 0.01$, ***$P \leq 0.001$, ****$P \leq 10^{-4}$.

Figure 3 Evaluating the performance of binary movement state classifiers. We performed hyperparameter tuning on Linear discriminant analysis (LDA) classifiers using canonical power band (PB) features. (A) The optimal epoch durations were identified for single-site (STN/GPi, S1 or M1) and combined models using the area under the receiver operating characteristic (AUC). (B) These models were then tested on a holdout set for each patient. We also evaluated the performance of classifiers trained on personalized features. (C) We performed principal component analysis (PCA) and identified the optimal number of PC features for each classifier. (D) The AUCs of the personalized classifiers with PC features were computed on the holdout set. Permutation feature importance was performed to quantify the unique contributions of each (E) site (STN/GPi, S1 or M1) and (F) canonical PB to the performance of the combined model. (G) Additional linear and non-linear models – Gaussian naïve bayes (GNB), k-nearest neighbors (KNN), random forests

(RF) and light gradient boosted machines (LGBMs) – were developed using all PSD features from each site, to avoid restricting the models to the six canonical PB features. *$P \leq 0.05$, **$P \leq 0.01$, ***$P \leq 0.001$, ****$P \leq 10^{-4}$.

Figure 4 Evaluating the performance of forearm movement speed regressors. Linear regression (LR) models were trained to predict continuous forearm speeds. (A) The optimal epoch durations were identified for single-site (STN/GPi, S1 or M1) and combined regressors were identified using Pearson *r* statistic values. (B) Evaluation of these LR models was performed on a holdout set. (C) Personalized features were developed using principal component analysis (PCA) and the optimal number of PC features for each regressor was determined. (D) The performance of the personalized single-site and combined regressors with PC features was compared using the holdout set. Permutation feature importance was computed for each (E) brain region and (F) canonical PB. (G) Additional linear and non-linear models – Bayesian ridge regression (BR), stochastic gradient descent (SGD), k-nearest neighbors (KNN), random forests (RF) and light gradient boosted machines (LGBMs) – were developed using the canonical PB features. *$P \leq 0.05$, **$P \leq 0.01$, ***$P \leq 0.001$, ****$P \leq 10^{-4}$.

Figure 5 Effects of stimulation on biomarkers of naturalistic movement. We computed the average normalized, flattened PSDs for the mobile and stationary states from the left STN of a single subject at two stimulation levels: (A) 0.0 mA and (B) 2.0 mA. The differences in spectral power across each canonical band were highlighted using different colors. We employed linear mixed models (LMMs) to investigate how the absolute Cohen's d effect size for each canonical power band varied across stimulation levels, which were treated as fixed effects. To visualize these relationships, we plotted the average absolute Cohen's d values across all patients for each stimulation amplitude in the following regions: (C) STN/GPi, (D) S1, and (E) M1. Additionally, LMMs were used to analyze variations in the area under the curve (AUC) for binary movement state classifiers, examining the effects of (F) the duration between sessions and (G) stimulation level. We also assessed changes in the *r* statistic for forearm movement speed regressors with respect to (H) the duration between sessions and (I) stimulation level. Figs. 5F–5I illustrate these relationships by plotting the average model performance across all patients against either the duration between sessions or the stimulation level. For all analyses presented in Figs. 5C–5I, individual patients and hemispheres were modeled as random effects in the respective LMMs.

Table 1 Patient demographics, stimulation settings and clinical information

Patient ID	Age, years; Sex	Dx, years	Stim target	Hem	Stim frequency, Hz	Stim levels, mA	UPDRS-III		Carbidopa-Levodopa (Daily dosage)
							OFF	ON	
Pat-01	60; M	13	STN	L	130	2.2–2.8	49	5	25–100 mg IR (5 times daily)
				R	130	2.7–3.5			
Pat-02	69; M	25	STN	L	130	1.9–2.5	45	22	50–200 mg CR (4 times daily)
				R	130	1.4–1.6			
Pat-03	46; M	10	STN	L	130	1.5–2.2	41	10	25–100 mg IR (2 times daily)
				R	130	1.5–2.2			
Pat-04	63; M	18	STN	L	130	2.9	44	11	25–100 mg IR (5 times daily)
				R	130	1.9–2.0			
Pat-05	76; M	13	STN	L	130	1.9–2.2	29	12	25–100 mg IR (4 times daily)
				R	130	1.0			
Pat-06	65; M	11	STN	L	130	0.0–2.9	35	12	24–95 mg ER (4 times daily)
				R	130	0.0–3.1			
Pat-07	48; M	17	STN	L	130	0.0–1.9	32	5	24–95 mg IR (5 times daily)
				R	130	0.0–1.9			
Pat-08	69; M	14	STN	L	130	0.0–2.6	30	7	24–95 mg ER (5 times daily)
				R	130	0.0–2.4			
Pat-09	62; M	16	STN	L	130	0.0	34	9	25–100 mg IR (5 times daily)
				R	130	0.0			
Pat-10	75; M	19	STN	L	130	0.0	31	10	49–195 mg ER (4 times daily)
				R	130	0.0			
Pat-11	79; M	14	STN	L	159	3.4	37	24	36–145 mg ER (4 times daily)
Pat-12	34; F	18	STN	R	167	1.2–2.2	61	16	25–100 mg IR (5 times daily)
Pat-13	53; M	14	GPi	L	130	0.0–1.1	49	19	49–195 mg ER (4 times daily)
				R	130	0.0–1.6			
Pat-14	71; M	15	GPi	L	179	3.7	66	24	25–100 mg IR (4 times daily)
				R	179	2.8			
Pat-15	69; M	10	GPi	L	149, 188	0.0–3.9	31	15	25–100 mg IR (5 times daily)

Dx = disease duration; STN = subthalamic nucleus; GPi = globus pallidus internus; L = left hemisphere; R = right hemisphere; PoG = post-central gyrus; PrG = pre-central gyrus; SFG = superior frontal gyrus; MFG = medial frontal gyrus; SPL = superior parietal lobe; UPDRS = Unified Parkinson's Disease Rating Scale; ER = extended release; IR = immediate release; CR = controlled release.

Table 2 Average group-level performance of linear models from each brain region

Metric	Combined	STN/GPi	S1	M1
Mean ± SEM Classifier Performance				
AUC	0.84 ± 0.01	0.72 ± 0.02	0.80 ± 0.02	0.80 ± 0.02
Balanced Accuracy	0.76 ± 0.01	0.66 ± 0.02	0.73 ± 0.01	0.73 ± 0.02
F1 Score	0.80 ± 0.02	0.71 ± 0.02	0.77 ± 0.02	0.78 ± 0.02
PPV	0.86 ± 0.03	0.79 ± 0.04	0.84 ± 0.03	0.84 ± 0.03
Sensitivity	0.75 ± 0.02	0.66 ± 0.02	0.72 ± 0.02	0.73 ± 0.02
Specificity	0.77 ± 0.01	0.67 ± 0.02	0.74 ± 0.01	0.74 ± 0.02
Mean ± SEM Regressor Performance				
r statistic	0.64 ± 0.03	0.41 ± 0.04	0.58 ± 0.03	0.58 ± 0.04
MSE	0.41 ± 0.02	0.57 ± 0.04	0.48 ± 0.03	0.48 ± 0.02

SEM = standard error of the mean; AUC = area under receiver operating characteristic curve; PPV = positive predictive value; r statistic = Pearson correlation coefficient between true and predicted values; MSE = mean squared error.

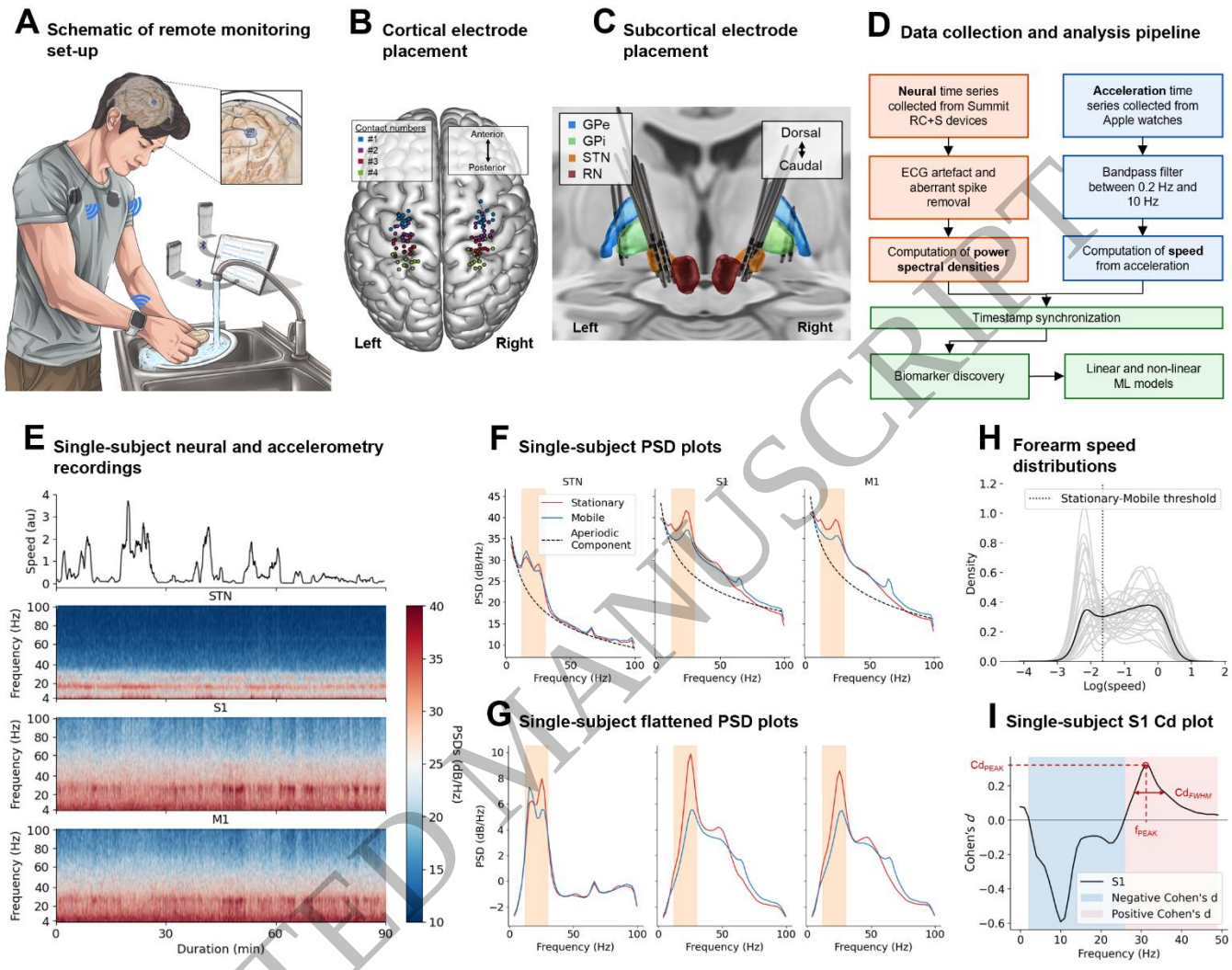

Figure 1
183x143 mm (x DPI)

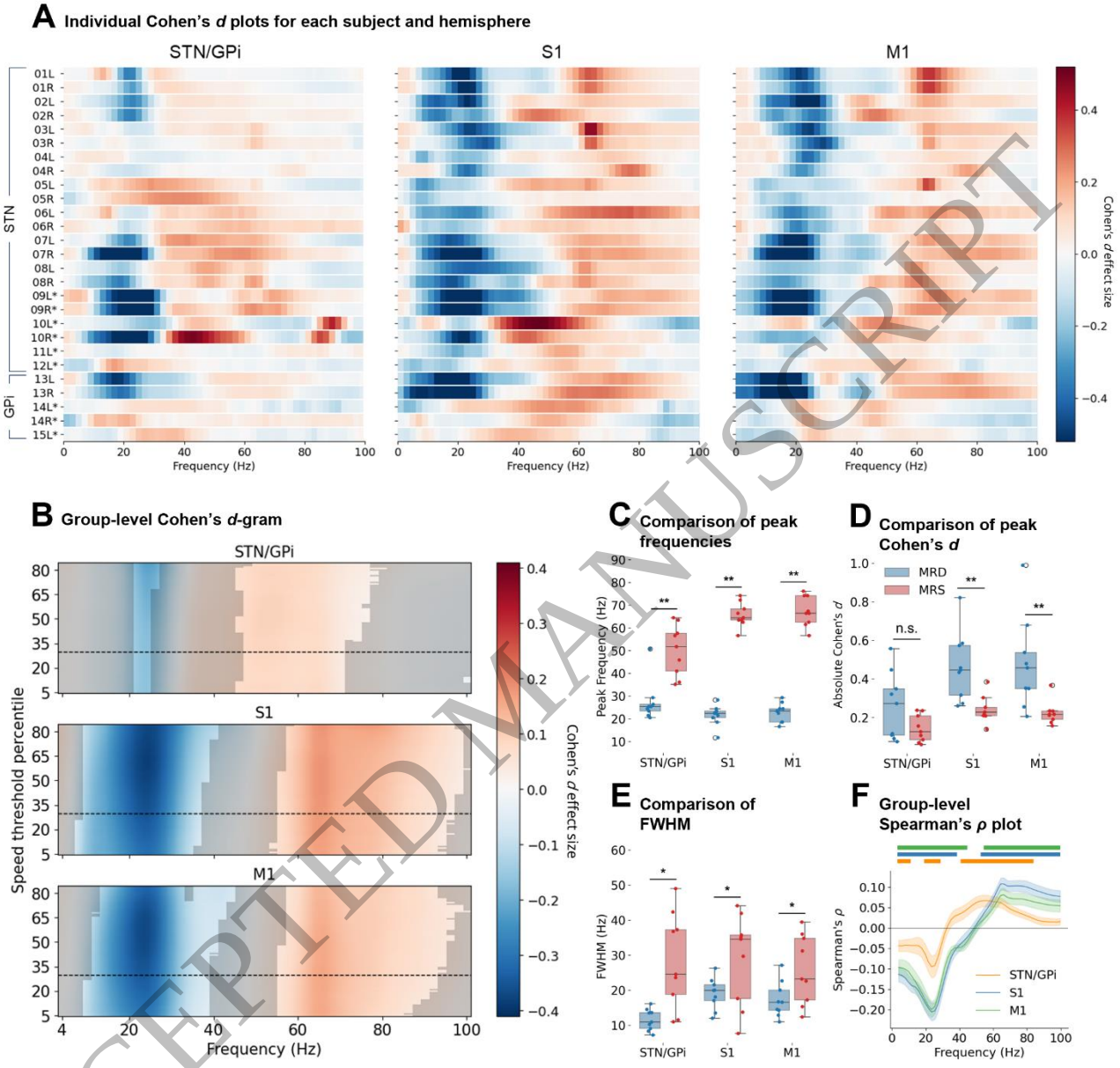

Figure 2
171x165 mm (x DPI)

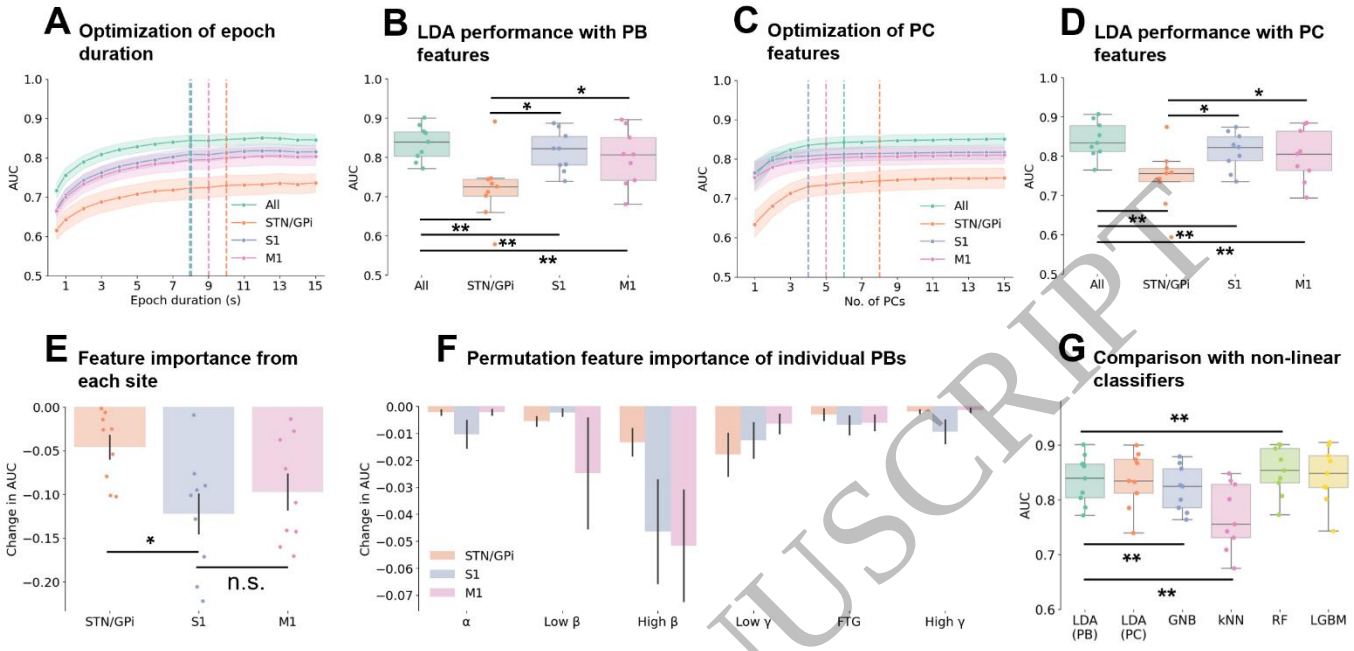

Figure 3
183x87 mm (x DPI)

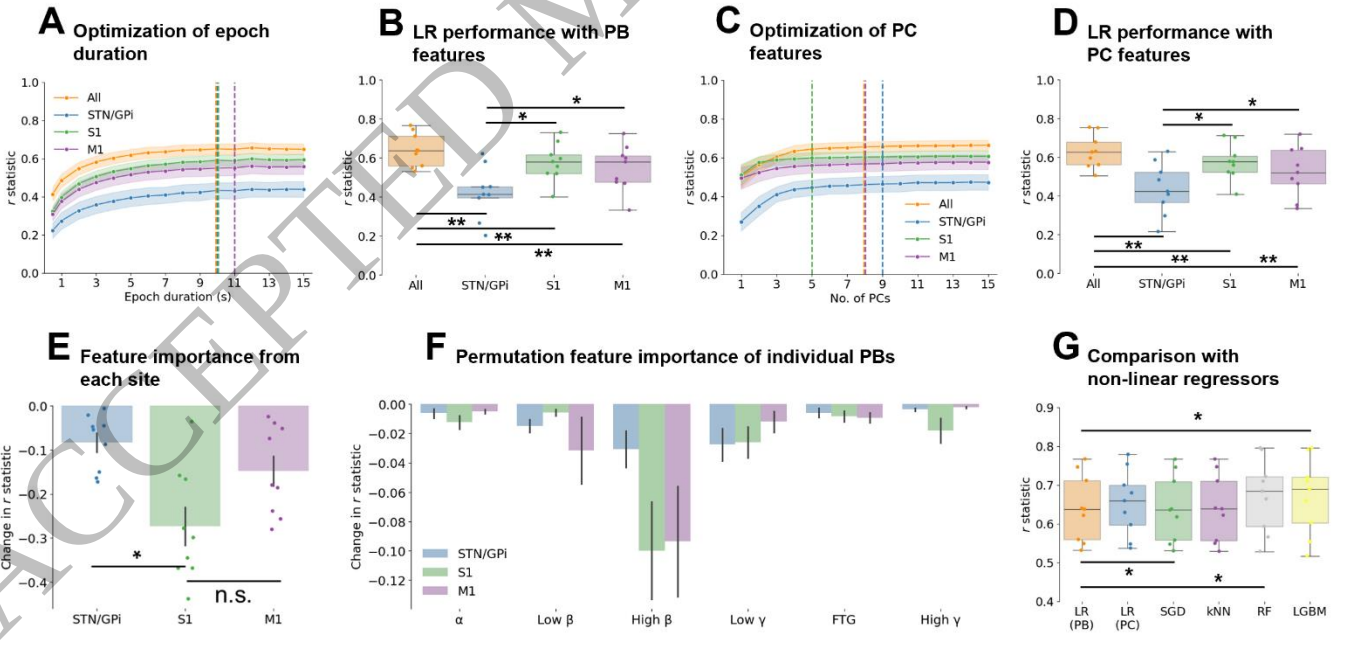

Figure 4
179x88 mm (x DPI)

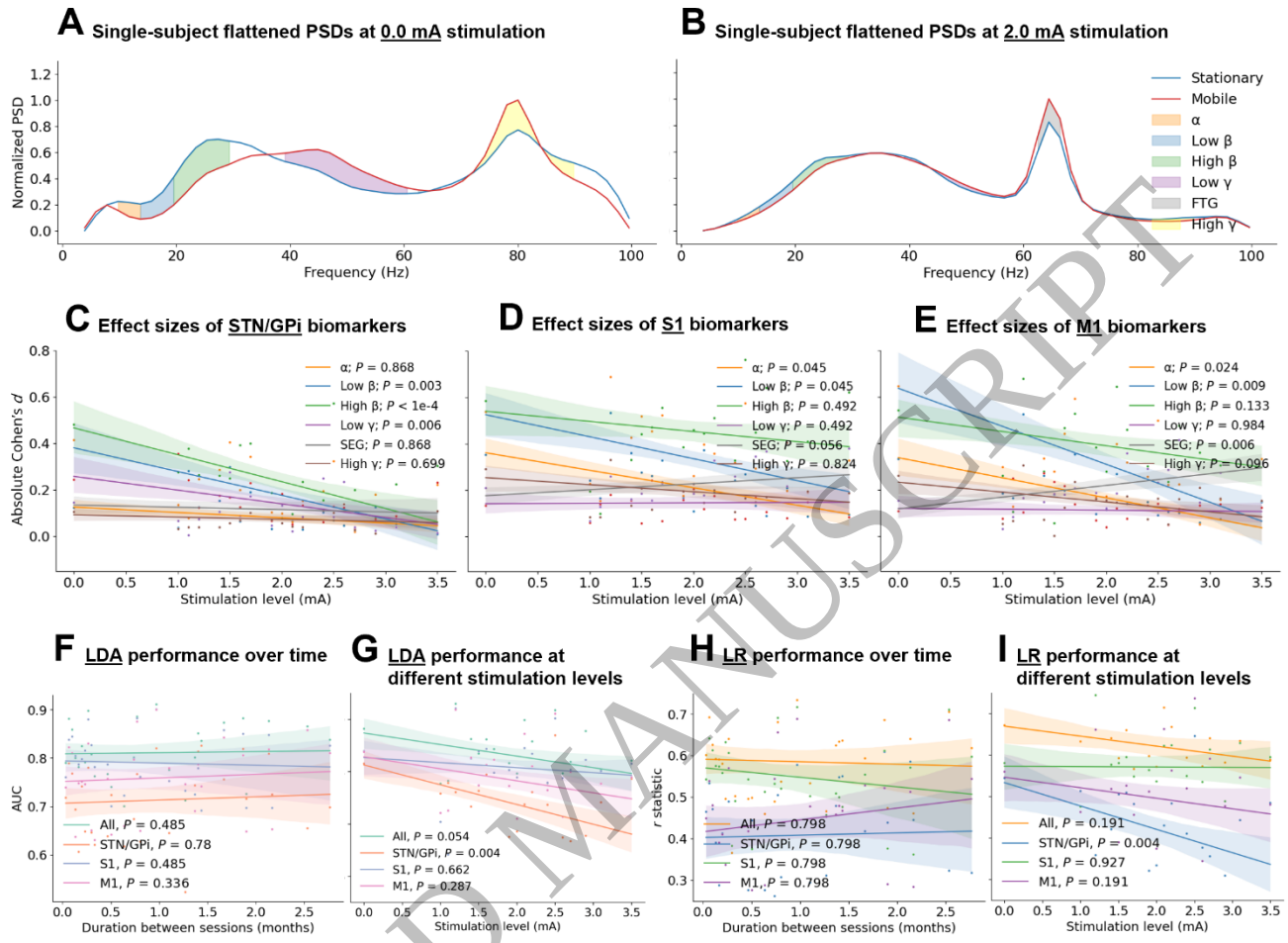

Figure 5
178x129 mm (x DPI)